phys. stat. sol. (a) **191**, No. 2, 391–408 (2002)

Positron-Lifetime Investigation of Thermal Stability of Ultra-Fine Grained Nickel

J. Čížek[1]) *) (a), I. Procházka (a), M. Cieslar (a), I. Stulíková (a), F. Chmelík (a), and R. K. Islamgaliev (b)

(a) Faculty of Mathematics and Physics, Charles University, V Holešovičkách 2, 180 00 Prague 8, Czech Republic

(b) Institute of Physics of Advanced Materials, Ufa State Aviation Technical University, Ufa 450000, Russia

(Received October 16, 2001; in revised form January 30, 2002; accepted January 31, 2002)

Subject classification: 61.46.+w; 61.72.–y; 78.70.Bj; 79.60.Jv

Thermal stability of ultra-fine grained (UFG) nickel (mean grain size 114 nm) prepared by high pressure torsion was studied by means of positron-lifetime spectroscopy (PLS) combined with TEM. The experimental results obtained by PLS are interpreted using the diffusion trapping model, which allows for determination of important physical parameters characterizing the specimens. The microstructure of the material studied is strongly inhomogeneous. The grain interiors with low dislocation density are separated by distorted regions with high numbers of dislocations. We have found that positrons are trapped at dislocations inside the distorted regions and in the microvoids situated inside the grains. Structure evolution with increasing temperature was studied in details using isochronal annealing of the specimen. We have found that recovery of the UFG structure involves the abnormal grain growth followed by further recrystallization in the whole volume of samples. It was shown that PLS is sensitive to structure changes, caused by the magnetostriction phenomenon.

1. Introduction

Recently it has been found that techniques based on severe plastic deformation can be used to produce ultra-fine grained (UFG) materials. Particularly high presure torsion (HPT) allows for preparation of UFG materials with a mean grain size about 100 nm [1, 2]. Similarly to nanocrystalline (NC) materials prepared e.g. by the gas condensation technique (GCM) [3], the UFG materials exhibit a number of unusual physical and mechanical properties and become, therefore, highly attractive for materials science. Moreover, the UFG materials appeared to be promising for further industrial applications. In particular the UFG materials are characterized by high srengthened state [4] and enhanced ductility and superplasticity [2, 5]. In addition, they exhibit changes of usually structure-insensitive parameters as elastic moduli, Curie and Debye temperature, saturation magnetization etc. [2, 6]. These properties are induced by significant volume fraction of grain boundaries (GBs) in the UFG materials.

However, the UFG structure becomes usually unstable at elevated temperatures. As the advantageous properties are bound to the UFG structure, information about thermal stability of these materials is very valuable. Moreover, the UFG structure repre-

[1]) Corresponding author; Tel.: +420-2-21912788; Fax.: +420-2-21912567; e-mail: jcizek@mbox.troja.mff.cuni.cz

*) Present address: Institut für Materialphysik, Universität Göttingen, Hospitalstr. 3–7, 37073 Göttingen, Germany, Tel.: 49-551-395302; Fax: 49-551-395012.

 0031-8965/02/19106-0391 $ 17.50+.50/0

sents highly non-equilibrium solid state, therefore, its evolution with temperature is very interesting. Clearly, detailed information about thermal stability of the UFG materials is necessary also for their further exploitation in industry.

In recent years, several works [7–12] have been devoted to investigation of thermal evolution of structure occurring in UFG material during heating. These investigations have revealed that recovery of UFG structure involves grain growth and relaxation of a non-equilibrium defect structure of specimens. The processes, which take place during isochronal annealing of UFG Cu and Ni prepared by HPT have been studied by TEM, electrical resistometry, microhardness, DSC and XRD [7]. These investigations have revealed that significant recovery of electrical resistivity and relaxation of elastic strains precedes the grain growth observed at 175 °C in the case of UFG Ni. The decrease of electrical resistivity, which occurs prior to the grain growth, is caused by recovery of defects and relaxation of elastic strains [7].

Thus, recovery of defects interferes with the grain growth during thermal evolution of UFG structure. It is, therefore, important to have separate information regarding behavior of defects with increasing temperature. Positron lifetime spectroscopy (PLS) is a well established technique for investigation of open-volume defects in solids [13]. Thus, PLS measurement correlated with other techniques is an ideal tool for investigation of evolution of defect structure of UFG materials.

It is known that the UFG materials prepared by HPT exhibit microstructure with large angle missorientation of neighboring grains [1, 7]. The grain interiors (non-distorted regions) almost free of dislocations are separated by distorted layers along GBs with high dislocation density and elastic strains [1]. Our investigations [9, 10] of thermal stability of UFG Cu by means of PLS correlated with TEM and XRD have revealed two types of defects present in this material: (i) dislocations situated in the distorted regions along GBs and (ii) microvoids with a size comparable to a few vacancies distributed homogeneously throughout the grains. In the case of UFG Cu we have found that isolated dislocation-free grains are formed in the deformed matrix (abnormal grain growth) with increasing temperature prior to the recrystallization [10]. Recovery of the microvoids takes place during the abnormal grain growth as well as due to the recrystallization. At the same time the mean size of the microvoids increases. It is assumed that some size distribution of the microvoids is present in the UFG Cu and only the largest ones from this distribution survive in the recrystallized specimen [10].

The comparison of available works dealing with thermal evolution of UFG structure [7–11] indicates that thermal stability of the UFG metals depends substantially on the initial grain size and the selected materials.

It is highly interesting whether the recovery of the UFG structure is made by similar processes also in UFG metals other than Cu. Thus, we have chosen UFG Ni in the present work, which is of great interest due to its ferromagnetic properties. An increasing number of GB dislocations was found on Ni step-by-step isochronaly annealed above Curie temperature $T_c = 358\,^{\circ}\mathrm{C}$, which is reflected by increase of electrical resistivity [7]. This phenomenon is caused by magnetostriction during quenching of specimens [14] and may lead to a significant difference between recovery processes in UFG Cu and Ni.

The aim of the present work is investigation of the thermal evolution of the structure of UFG Ni prepared by HPT. The structure changes and recovery of defects was studied by PLS correlated with TEM. The investigation was performed on the same UFG Ni samples on which TEM, electrical resistivity, microhardness, DSC and XRD meas-

urements were made in Ref. [7]. Thus, the results of our measurements obtained in the present work can be directly correlated with those obtained by other techniques in Ref. [7]. We developed a model for positron behavior in the UFG materials [10], which takes into account their specific structure, and allows for determination of physical parameters as the mean size of the non-distorted regions (the mean size of coherent domains), the volume fraction of the distorted regions, the dislocation density, and the concentration of microvoids, from experimental positron-lifetime spectra. This model called hereafter diffusion trapping model was successfully used in investigation of thermal stability of UFG Cu [10] and was applied in the present work also on UFG Ni.

2. Experimental

2.1 Specimens

In order to fabricate the UFG structure the Ni (99.98%) specimens were subjected to HPT under pressure of 6 GPa up to logarithmic degree of deformation $e = 7$ [1]. The deformation was performed at room temperature. The mean grain size of 114 nm in the as-prepared UFG Ni was determined by TEM [7]. The UFG specimens were disk shaped with diameter 10 mm and thickness 0.25 mm.

After characterization of the as-prepared state, the specimens were subjected to isochronal annealing with an effective heating rate of 1 °C/min (in steps 30 °C/30 min). The annealing was carried out in silicon oil base up to 250 °C and in vertical furnace with protective argon atmosphere above this temperature. Each annealing step was finished by rapid quenching into water of room temperature. The PLS and TEM measurements were carried out at room temperature.

2.2 Positron-lifetime spectroscopy

Positron-lifetime spectrometer similar to the fast–slow one described in Refs. [15, 16] was employed in the present work. The spectrometer was modified recently with purpose to enhance coincidence count rate keeping simultaneously the excellent timing resolution (for details see Refs. [16, 17]). The main improvement with respect to the device [15] consisted in selection of the coincidence events by means of summing the energy signals as described in Refs. [16, 17]. The timing resolution of the spectrometer was 150 ps (FWHM) for ^{22}Na at a typical coincidence counting rate of 75 s^{-1}. A ^{22}Na positron source of activity of $\sim$1.3 MBq sealed between two mylar foils of thickness of 2 μm was used. At least 10^7 counts were collected in each positron-lifetime spectrum. Measured spectra were decomposed by means of maximum-likelihood procedure [18] into up to five exponential components. The time-resolution function of the spectrometer was considered as a sum of the three gaussians and was fitted simultaneously with the other parameters (for details see Refs. [16, 18]).

2.3 Transmission electron microscopy

Observations of microstructure were performed on the JEOL 2000 FX electron microscope operating at 200 kV with EDX system LINK AN 10000. Thin foils for TEM were electropolished in a twin-jet device TENUPOL 2. The electropolishing was performed in 30% solution of HNO_3 at −20 °C.

3. Results and Discussion

3.1 As-prepared state

The bright field TEM image of as-prepared specimen is shown in Fig. 1. The mean grain size of 120 nm was found in agreement with Ref. [7]. As one can see in Fig. 1, the specimen exhibits fragmented structure with strongly inhomogeneous distribution of dislocations. The grain interiors almost free of dislocations are separated by distorted regions with high dislocation density, see Fig. 1a. The electron diffraction pattern, see Fig. 1b, testifies high-angle misorientation of neighboring grains. "Diffusion contrast" of GBs, see Fig. 1a, indicates non-equilibrium state of majority of GBs and existence of elastic stresses, which are caused by the non-equilibrium GBs.

The positron-lifetime spectrum of as-prepared specimen is well fitted by two exponential components (except of the source contribution) with lifetimes $\tau_2 = (157 \pm 1)$ ps and $\tau_3 = (336 \pm 8)$ ps, respectively. Lifetimes of both the components lie substantially above the Ni bulk lifetime $\tau_B = 108$ ps [19]. It clearly indicates that both the components come from positrons trapped at defects. The lifetime τ_2 is slightly lower than the lifetime of positrons trapped in Ni monovacancies $\tau_{1v} = 180$ ps [20], which is typical for the lifetime of positrons trapped at dislocations [21]. Note that the dislocation line itself represents only a shallow trap for positrons (positron binding energy < 0.1 eV). It is not compatible with the lifetimes found in deformed metals, which are only slightly shorter than those for monovacancies (positron binding energy ≈ 1 eV) [21]. Thus, it is generally accepted [21–23] that positrons trapped at a dislocation line diffuse quickly along the line and are eventually trapped at point defects associated with the dislocation as a vacancy bound to dislocation or jog at dislocation. Indeed, the lifetime of positrons trapped in a vacancy bound to dislocation in Ni was calculated to be about 160 ps [24]. Moreover, a component with lifetime (157 ± 2) ps was found experimentally on plastically deformed Ni [25]. For simplicity in the following text the statement "positron trapped at dislocation" will mean the process involving temporally trapping of a positron in the dislocation line and its final annihilation in a point defect associated with the dislocation as was explained above.

TEM investigations of UFG Ni have revealed a high number of dislocations situated inside the distorted layers along GBs. Thus, it is natural to attribute the first component

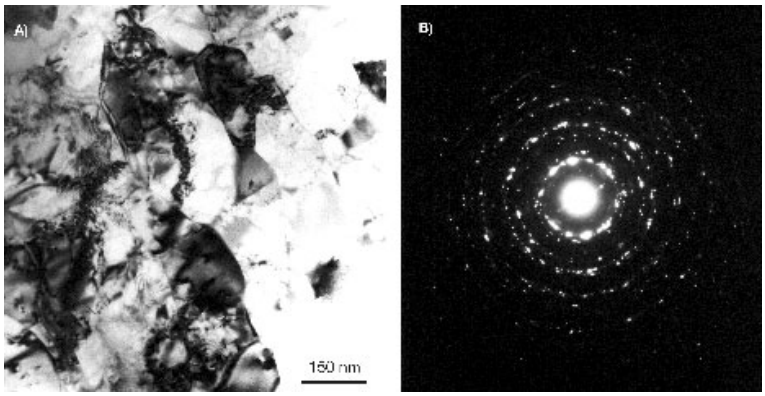

Fig. 1. a) Bright field TEM image and b) diffraction pattern of the as-prepraed UFG Ni

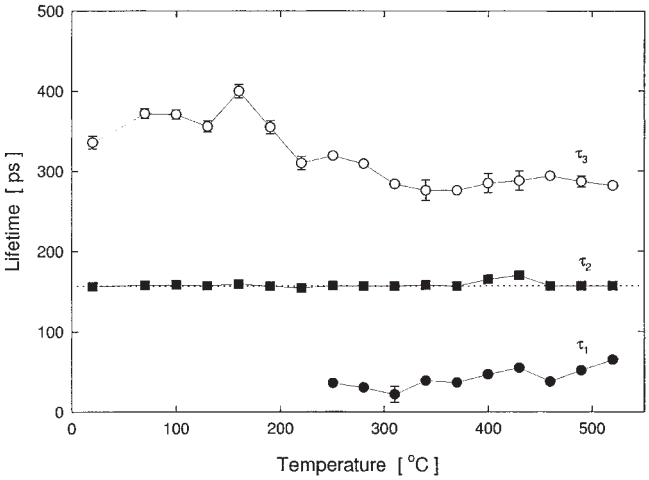

Fig. 2. Lifetimes of the components resolved in positron-lifetime spectra as a function of annealing temperature. The lifetime τ_2 exhibits only statistical fluctuations around the mean value of 157 ps, which is indicated in the figure by the dotted line

with lifetime τ_2 to positrons trapped at dislocations inside the distorted regions. The relative intensity of this component is 80%, i.e. the majority of positrons in the as-prepared specimen annihilates from trapped state at dislocations.

Vacancies in Ni become mobile at 100 °C [26, 27]. Not only a remarkably shorter lifetime $\tau_2 = 157$ ps, but also a relatively high thermal stability of this component, see Figs. 2, 3, and in particular no change of τ_2 after annealing above 100 °C indicate that the contribution of single vacancies to this component is negligible. It means that in the UFG Ni, vacancies introduced into the material due to plastic deformation are recovered even at room temperature probably due to higher deformation energy stored in the UFG material and, thereby, also higher driving force for recovery of non-equilibrium defects.

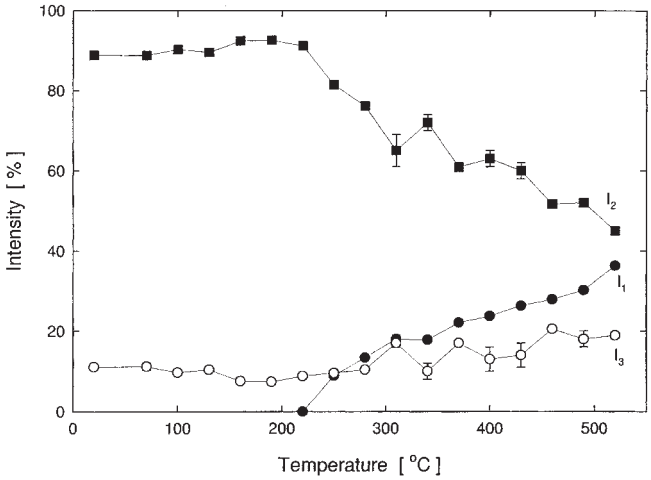

Fig. 3. Temperature dependence of relative intensities of spectral components

The component with lifetime τ_3 (relative intensity 20%) comes from positrons trapped at larger defects with free volume comparable to that of a few monovacancies. In similar manner as in the case of UFG Cu [10], we attribute this component to positrons trapped in microvoids distributed homogeneously throughout the grains. It is known from PLS studies of deformed Cu [28] that strong plastic deformation often introduces the microvoids into the specimen. Thus, the microvoids apparently were created in the UFG Ni due to severe deformation.

We note that a number of PLS studies of NC metals prepared by GCM have revealed also the existence of vacancy-like traps of positrons and some larger defects with a lifetime from 300 to 450 ps [29–32]. The larger defects in NC materials are attributed by most authors to defects situated at triple junctions of GBs (triple points) [29]. However, in the case of UFG materials the defects responsible for the lifetime τ_3 are situated inside grains [10].

One can easily estimate the trapping rate to defects situated in the triple junctions in NC and UFG materials. If we approximate a grain by a cube with side d, then there is one triple point per grain. Thus, atomic concentration of the triple points c_t can be expressed

$$c_t = \frac{1}{d^3 n_{Ni}} , \tag{1}$$

where n_{Ni} is the atom density, i.e. the number of atoms in a unit volume. Firstly we make this estimation for typical NC material with grain size $d = 10$ nm. In such a case we obtained $c_t = 1.1 \times 10^{-5}$ at.$^{-1}$. Further we assume that one defect is situated at each triple point. A free volume of these defects corresponds to that of ten vacancies, see Section 3.3. Under these assumptions, we can estimate the positron trapping rate K for these defects.

$$K \approx c_t n \nu_{1v} , \tag{2}$$

where $n = 10$ and ν_{1v} denotes the specific positron trapping rate for monovacancy. Hence, the specific trapping rate for a microvoid is assumed to be roughly proportional to the number of vacancies in the microvoid. Typically $\nu_{1v} = (10^{14}–10^{15})$ at. s^{-1} in metals [13]. Therefore, we used $\nu_{1v} = 5 \times 10^{14}$ at. s^{-1} in this estimation. For typical NC nickel, we obtained $K \approx 6 \times 10^{10}$s^{-1}. This trapping rate is comparable or higher than the bulk annihilation rate $\lambda_B = 1/\tau_B = 9.2 \times 10^9$ s^{-1}. Secondly we make the same estimation for typical UFG Ni with grain size $d = 100$ nm. For such material we obtained $K \approx 6 \times 10^7$ s^{-1}, which is more than two orders of magnitude lower than the bulk annihilation rate. Thus, in contrary to NC materials, the concentration of defects situated in the triple points is too low to represent noticeable contribution to positron-lifetime spectra in UFG materials. Hence, this simple estimation supports our interpretation regarding the microvoids in the UFG Ni.

Note that a lifetime of 230 ps was reported by some authors for deformed Ni [33]. This lifetime is certainly too high to be attributed to positrons trapped at dislocations. Clearly, it is an effective value, which involves contribution of positrons trapped at dislocations as well as those trapped in microvoids.

Hence, we conclude that similarly to UFG Cu, positrons are trapped at dislocations inside the distorted regions and in the microvoids distributed homogeneously throughout the grains. The fact that no contribution of free positrons was resolved in the posi-

tron-lifetime spectrum, i.e. all positrons are trapped at defects in the as-prepared state, is not surprising as most of the positrons are trapped at dislocations inside the distorted regions along GBs and the mean grain size of 114 nm is comparable with the mean positron diffusion length $L_+ = 150$ nm in defect free Ni.

3.2 Isochronal annealing

The mean lifetime $\overline{\tau}$ is a robust statistic parameter, which is not affected by the assumed number of components or constraints made in the fit of the positron-lifetime spectrum. Thus, it is reasonable to use $\overline{\tau}$ firstly as an integral characteristics of evolution of the UFG structure with temperature. Temperature dependence of $\overline{\tau}$ for the UFG Ni is shown in Fig. 4. One can see in Fig. 4 that no essential change of $\overline{\tau}$ takes place up to 160 °C. The main decrease of $\overline{\tau}$ occurs in the temperature region from 190–340 °C. An interesting feature is that from 350 °C $\overline{\tau}$ starts to increase again, see Fig. 1, and reaches its maximum at 430 °C. Such kind of behavior was not observed on UFG Cu [10]. Above 430 °C $\overline{\tau}$ decreases back and remains roughly constant at higher annealing temperatures.

It is clear from the temperature dependence of $\overline{\tau}$ that the main recovery of defects occurs between 190 and 340 °C. The increase of $\overline{\tau}$ from the Curie temperature (358 °C) is most probably caused by magnetostriction phenomena during quenching, which is responsible also for the observed increase of electrical resistivity above the Curie temperature [7, 12]. The increasing number of dislocations in the vicinity of GBs was observed in quenched UFG Ni annealed above the Curie Temperature [12].

More detailed information about processes, which take place during the recovery of the UFG structure can be obtained from the decomposition of positron-lifetime spectra to individual components. The positron-lifetime spectra of UFG Ni are well fitted by two exponential components with the lifetimes τ_2 and τ_3, respectively up to temperature 220 °C. Above 220 °C, an additional component with lifetime τ_1 appears in the positron-lifetime spectra. Thus, above 220 °C, the positron-lifetime spectra are well fitted by three exponential components. Temperature dependencies of the lifetimes τ_1,

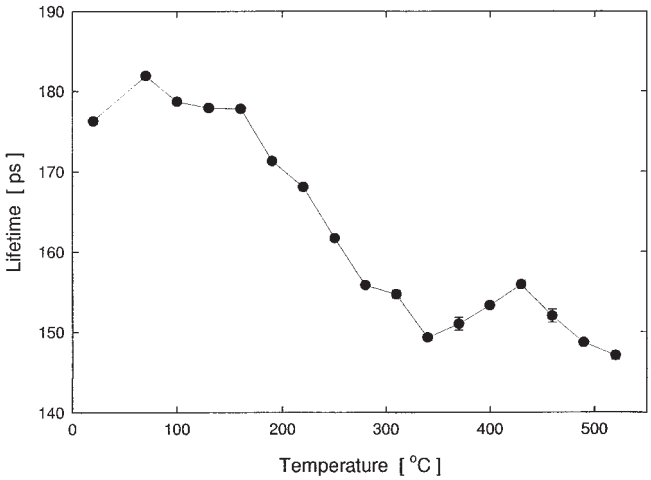

Fig. 4. Temperature dependence of the mean lifetime $\overline{\tau}$

τ_2 and τ_3 and corresponding relative intensities are shown in Fig. 2 and Fig. 3, respectively. As one can see in Fig. 2 the lifetime τ_1 lies well below 100 ps and therefore represents a contribution of free positrons. The lifetime τ_2 does not exhibit any change with annealing temperature except of statistical fluctuations around the mean value of 157 ps (shown by the dotted line in Fig. 2). On the other hand, the lifetime τ_3 increases (up to 190 °C), while at higher temperatures τ_3 decreases (up to 300 °C), see Fig. 2. Above the Curie temperature τ_3 exhibits slight gradual increase. The decrease of τ_3 with temperature in the interval of 190–300 °C is a rather surprising effect as in the case of UFG Cu the lifetime τ_3 exhibited an opposite behavior [10].

The relative intensity I_2 remains constant to 130 °C, then it exhibits a slight increase in the temperature interval from 130–200 °C, see Fig. 3. This slight increase is correlated with a decrease of I_3 in this temperature range. This effect indicates abnormal grain growth, which takes place also in UFG Cu prior to recrystallization [10, 11]. Isolated recrystallized grains appear in the practically unchanged deformed matrix. Similarly to the case of UFG Cu [10], the abnormal grain growth leads to a slight decrease of the number of the microvoids reflected by a decrease of I_3, while the dislocation density remains unchanged. Hence, the number of microvoids in the isolated recrystallized grains is lower.

A bright-field TEM image of the UFG Ni specimen annealed up to 190 °C is shown in Fig. 5a. The corresponding diffraction pattern is shown in Fig. 5b. The isolated recrystallized grains are present in the deformed matrix in the specimen annealed up to 190 °C, see Fig. 5a. It indicates the abnormal grain growth in this temperature interval. It was estimated that the fraction of abnormaly grown grains is about 5% at 190 °C. The recrystallized isolated grains are almost free of dislocations and contain the annealing twins.

Above 200 °C I_2 decreases dramatically, see Fig. 3, which indicates recovery of dislocations. The slope of this decrease changes at 300 °C, above this temperature I_2 continuously decreases more moderately. Above 200 °C, where the radical decrease of I_2 starts, the free positron component with relative intensity I_1 appears in the positron-lifetime spectrum. A comparison of PLS and TEM observation leads to the conclusion that the radical decrease of $\bar{\tau}$ and I_2, see Figs. 3 and 4, respectively, in the temperature interval

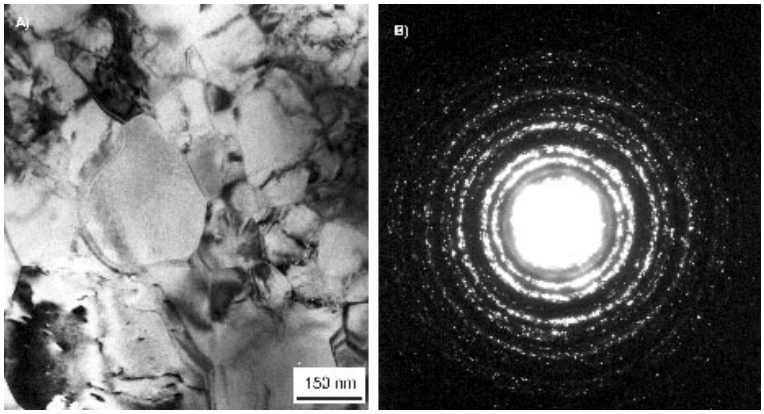

Fig. 5. a) Bright field TEM image and b) diffraction pattern of UFG Ni annealed up to 190 °C

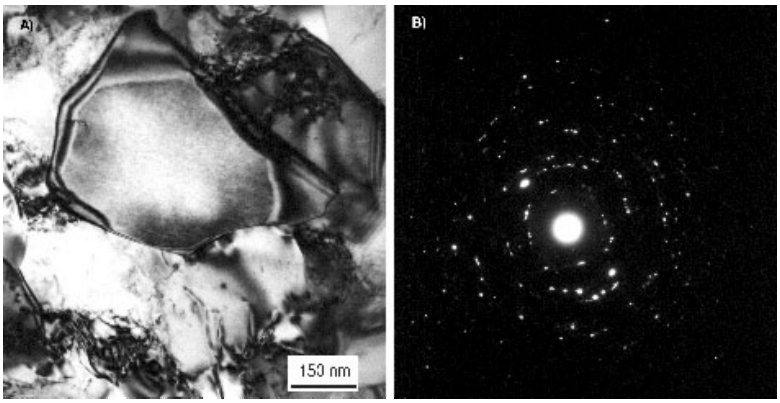

Fig. 6. a) Bright field TEM image and b) diffraction pattern of UFG Ni annealed up to 250 °C

200–400 °C takes place due to recrystallization. Below the term recrystallization will be used for description of the structure changes in the temperature interval 200–400 °C. This term will be associated with grain coarsening in the whole volume of sample observed after the abnormal grain growth. The distorted regions with high dislocation density are consumed by recrystallized grains, leading to a substantial decrease of dislocation density.

Bright field TEM image and the electron diffraction pattern of the specimen annealed up to 250 °C is shown in Figs. 6a and b, respectively. The specimen annealed up to 250 °C is characterized by a recrystallized structure with isolated regions of a non-recrystallized initial deformed matrix, see Fig. 6a. The fraction of recrystallized volume is about 80% at 250 °C. Similarly to the case of the abnormal grain growth, the annealing twins were found inside the recrystallized grains.

The fraction of non-recrystallized volume decreases to only about 1% at the specimen annealed up to 380 °C. The bright-field TEM images for the specimen annealed up to 380 and 400 °C are shown in Figs. 7a and b, respectively. The specimen annealed up to 400 °C exhibits a fully recrystallized structure. The presence of the annealing twins in

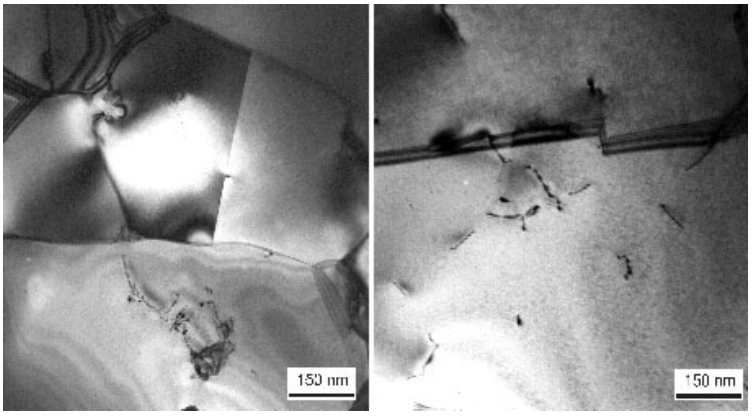

Fig. 7. Bright field TEM image of the UFG Ni specimen annealed up to a) 380 °C and b) 400 °C

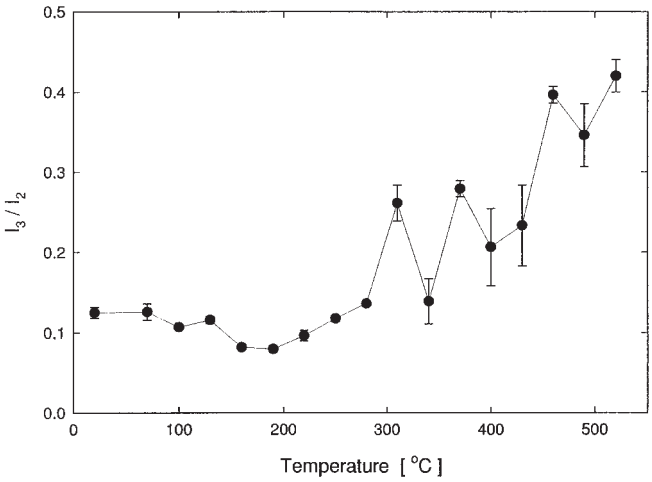

Fig. 8. Temperature dependence of the ratio I_3/I_2

the recrystallized grains is a typical feature of the recrystallized sample similarly as in the case of UFG Cu [10].

Note that the same sequence, i.e. the abnormal grain growth followed by the recrystallization was also found in UFG Cu [10, 11]. Further decrease of I_2 above 400 °C is probably due to growth of recrystallized grains.

The relative intensity I_3 corresponding to the microvoids remains virtually unchanged or even slightly increases during the recrystallization. At the same time the corresponding lifetime τ_3 decreases during the recrystallization. Both these trends are opposite to those observed during the recrystallization in UFG Cu [10]. Hence, in contrary to UFG Cu, the larger microvoids in Ni seem to decay to smaller ones during the recrystallization. The decrease of the mean size of microvoids is reflected by the decrease of τ_3, while the increase of their concentration is reflected by the increase of I_3, see Figs. 2 and 3, respectively.

Above the Curie temperature (358 °C), the lifetime τ_3 slightly increases, which indicates the increase of the mean size of the microvoids. The relative intensity I_3 exhibits also moderate increase above the Curie temperature.

An interesting picture about the evolution of both kinds of defects with increasing temperature may be seen in Fig. 8, where temperature dependence of the ratio I_3/I_2 is shown. The two different processes, i.e. the abnormal grain growth and the recrystallization, are indicated by a different slope of the I_3/I_2 ratio dependence. Clearly, after initial decrease in the temperature interval of 130–200 °C due to the abnormal grain growth, the ratio I_3/I_2 continuously increases above 200 °C. It indicates that in the UFG Ni the microvoids are more stable with respect to temperature than dislocations. Similar behavior of the relative intensities of vacancy-like and larger defects with temperature was observed also in NC Cu prepared by GCM [30].

3.3 Microvoids

In the present section a special attention is focused to the microvoids. We note that important profit of using PLS study on the present material consists in its ability to

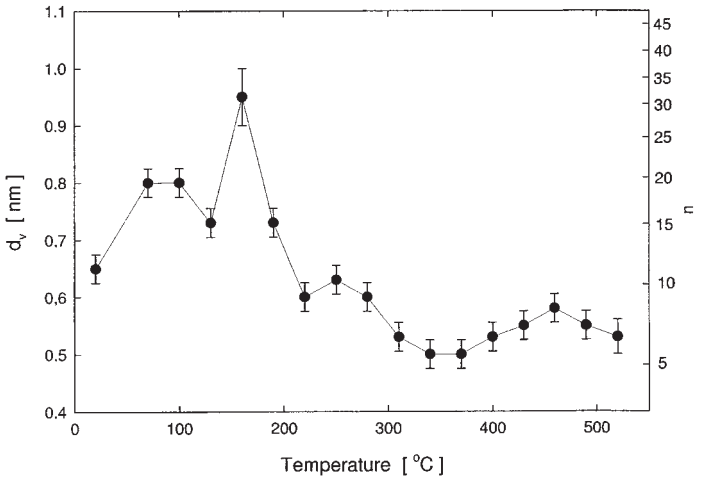

Fig. 9. Diameter d_v of the microvoids as a function of temperature. The diameter d_v was calculated from τ_3 using results of theoretical calculations [34]. The number of vacancies n, from which the microvoid consists is shown on the left vertical axis

bring valuable information regarding the microvoids (concentration, mean size), which can hardly be provided by other techniques due to their small size. The lifetime τ_3 of positrons trapped in the microvoids brings information about the size of the microvoids. The dependence of positron lifetime on the size of a vacancy cluster was calculated in Ref. [34] for Ni. Using the results of this calculation, one can determine from the lifetime τ_3 the linear size d_v (diameter) of the microvoids as a function of annealing temperature. This dependence is plotted in Fig. 9. In addition to the diameter d_v of microvoid, the number of vacancies n making up the microvoid, is shown in Fig. 9. We assume that some size distribution of the microvoids is present in the UFG specimen. Then the diameter d_v represents the center-of-mass of this distribution. In order to determine the shape of this distribution and its possible changes with temperature, additional PLS studies, which consider continuous distribution of positron lifetimes in decomposition of the experimental spectra, are required. An attempt to perform such analysis is currently in progress.

One can see in Fig. 9 that d_v exhibits firstly some increase, which may be caused by relaxation of the elastic strains. The maximum of d_v corresponds to 160 °C, when the abnormal grain growth occurs. A significant decrease of d_v occurs during the recrystallization (200–300 °C), see Fig. 9. This behavior can be explained only as decay of larger microvoids to smaller ones during the recrystallization. Above the Curie temperature (358 °C), d_v moderately increases.

Note that the mean diameter of the microvoids at 520 °C ($\approx$0.55 nm) is lower than the initial one ($\approx$0.65 nm), see Fig. 9. This feature is completely opposite to that observed in UFG Cu [10].

3.4 Application of the diffusion trapping model

In order to obtain more physical parameters related to the UFG structure of the studied specimen, we used the diffusion trapping model developed by us for the UFG

materials [10]. The model is completely described in Ref. [10]. Here we give only the assumptions of the model. We consider that UFG material consists of spherical non-distorted regions (grain interiors) with radius R separated by the distorted regions (distorted layers along GBs) of thickness δ. Positrons inside the distorted regions annihilate from trapped state at dislocations, while positrons inside the non-distorted regions annihilate as free or trapped in microvoids. Moreover, the free positrons inside the non-distorted regions diffuse throughout the specimen and may reach a distorted region and be trapped here. On the base of TEM investigations [7, 10], we use $\delta = 20$ nm. The positron diffusion coefficient for Ni is $D_+ = 2.2$ cm^{2}s^{-1} [35].

The application of the model leads to a diameter of the non-distorted region $2R$, which is shown as a function of temperature in Fig. 10. It should be pointed out that $2R$ does not correspond to the mean grain size obtained e.g. using TEM. It is due to a different definition of grain size, which is connected to a change of contrast in the TEM image inside the grain and at a GB. On the other hand, the size of the non-distorted region is correlated with a different dislocation density inside the distorted and the non-distorted regions. The mean size of the non-distorted regions $2R$ thus corresponds rather to the mean size of coherent domain determined by XRD [7], which is also directly connected to the dislocation density. It is known that in the UFG materials the mean size of a coherent domain determined by XRD is remarkably lower than the grain size obtained by TEM [7, 10]

The temperature dependence of the volume fraction η of the distorted regions is also shown in Fig. 10. Note that the model cannot be used when saturation trapping of positrons in defects occurs. Thus, in our case the model can be applied only to annealing temperatures above 200 °C.

Up to 250 °C, the mean size of the non-distorted regions $2R = (80 \pm 10)$ nm was obtained, see Fig. 10. As the deformed matrix remains practically unchanged during the abnormal grain growth, we assume that a similar value of $2R$ corresponds also to an as-

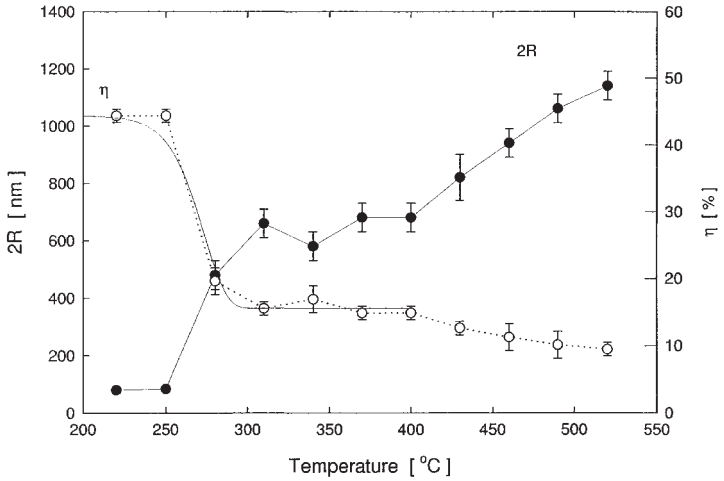

Fig. 10. Temperature dependence of the mean size of the non-distorted regions $2R$ ($-\bullet-$) and the volume fraction η ($\cdots\circ\cdots$) of the distorted regions obtained using the diffusion model. The smooth solid line represents the fit of temperature dependence of η using Eq. (7), see text

prepared state of the specimen. This value of $2R$ lies somewhere between the size of the coherent domain of 50 nm obtained using XRD and the grain size of 114 nm determined by TEM [7]. Thus, as expected the mean size of the non-distorted regions is smaller than the mean grain size determined by TEM. It should be pointed out that the mean size of the non-distorted regions and the mean grain size have to be distinguished only prior to the recrystallization. In the recrystallized specimen there is no difference between these two parameters.

During the recrystallization $2R$ abruptly increases by one order of magnitude, see Fig. 10. Above 350 °C, R exhibits further gradual increase, which indicates growth of the recrystallized grains.

The temperature dependence of the volume fraction η of the distorted regions determined using the diffusion model is shown in Fig. 10. One can see in Fig. 10 that η exhibits drastic decrease during the recrystallization because the distorted regions are consumed by the recrystallized grains. Further moderate decrease of η above 400 °C is connected to the growth of the recrystallized grains.

The increase of the volume fraction $X \equiv 1 - \eta$ of the recrystallized material with time t can be described by Göhler-Sachse's equation [36]

$$\frac{\mathrm{d}X}{\mathrm{d}t}\,\frac{1}{1-X} = K(T)\,(t - t_\mathrm{n})^{m-1}\,, \tag{3}$$

where t_n represents incubation time for nucleation and m is the kinetic parameter known from Avrami's equation [37]. The quantity K depends on the temperature T by Arrhenius equation

$$K = K_0 \exp\left(-\frac{Q}{kT}\right), \tag{4}$$

where K_0 is a temperature-independent constant, k denotes the Boltzman constant and Q represents the activation energy of the recrystallization. The specimen was isochronally annealed, therefore, the effective heating rate $v_\mathrm{a} = \mathrm{d}T/\mathrm{d}t$ remains constant. Thus, time in Eq. (3) may be expressed using temperature as

$$t = (T - T_\mathrm{s})/v_\mathrm{a}\,, \tag{5}$$

where T_s denotes the annealing temperature, when the recrystallization starts. Inserting the Eqs. (4) and (5) into Eq. (3), one obtains the following expression for the recrystallized fraction X:

$$1 - X = \exp\left(-K_0 \int \exp\left(-\frac{Q}{kT}\right)(T/v_\mathrm{a} - t_1)^{m-1}\,\mathrm{d}T\right), \tag{6}$$

where t_1 is another temperature-independent constant. In our case, the volume fraction of distorted regions, i.e. $1 - X$, decreases from initial value η_1 to final value η_2, see Fig. 10. Thus, it is necessary to re-scale Eq. (6), which leads to expression

$$\eta = (\eta_1 - \eta_2) \exp\left(-K_0 \int \exp\left(-\frac{Q}{kT}\right)(T/v_\mathrm{a} - t_1)^{m-1}\,\mathrm{d}T\right) + \eta_2\,, \tag{7}$$

where η is used instead of $1 - X$. The integral on the right side of Eq. (7) was solved numerically and the obtained function was fitted to the temperature dependence of η obtained from experiment (Fig. 10). The function obtained from the fit is plotted in

Fig. 10 by a solid line. One can see in Fig. 10 that the fitted function exhibits reasonable agreement with experimental points. The activation energy $Q = (1.4 \pm 0.1)$ eV ((130 ± 10) kJ mol^{-1}) was determined from the fit for the recrystallization. This value agrees with the activation energy of 126 kJ/mol for migration of equilibrium GBs in Ni [38]. The excelent agreement of the activation energies confirms that the recrystallization occurs in a temperature range from 200 to 400 °C in our specimen.

Using the diffusion model it is possible to calculate the trapping rates K_D and K_v for the components with lifetimes τ_2 and τ_3, respectively. Temperature dependencies of the trapping rates are plotted in Fig. 11. Regarding the trapping rate K_D, it exhibits a sharp increase during the recrystallization. It clearly indicates a change of type of trapping centers, which contributes to the second component with lifetime τ_2. As it was discussed in the preceeding text the distorted regions are consumed by the recrystallized grains during the recrystallization. As a result the mean dislocation density in the recrystallized specimen decreased below 10^{13} m^{-2} [7], which is close to the lower limit of sensitivity of PLS [39]. Thus, prior to the recrystallization the component with lifetime τ_2 comes from positrons trapped at dislocations. On the other hand, in the recrystallized specimen this component represents contribution of positrons trapped at equilibrium

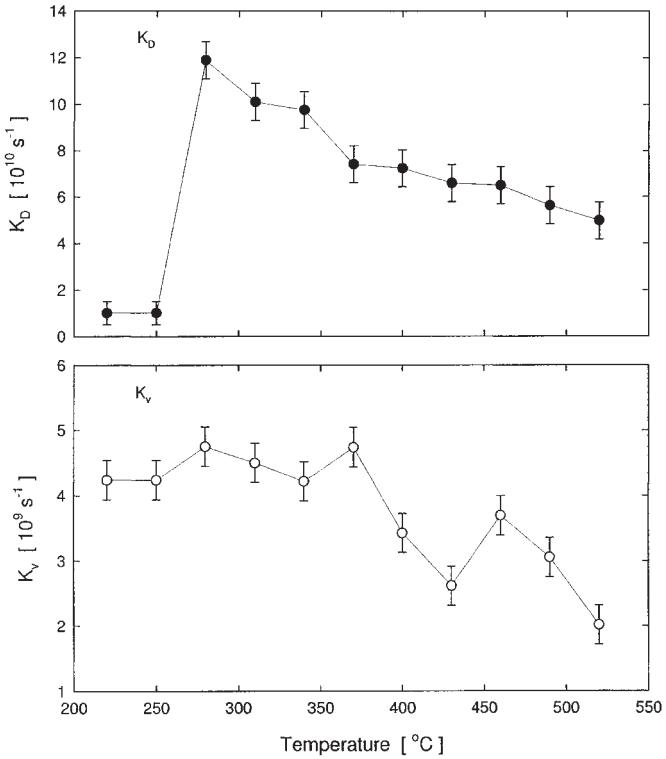

Fig. 11. Temperature dependence of positron trapping rates obtained from the diffusion model. The trapping rate K_D corresponding to the component with lifetime τ_2, which comes from positrons trapped at dislocations and GB, is plotted in the upper panel as a function of temperature. Temperature dependence of the positron trapping rate to microvoids, K_v, which belongs to the component with lifetime τ_3 is shown in the lower panel of the figure

high-angle GBs, which separate the grains. Further decrease of the trapping rate K_D, see Fig. 11, occurs due to the growth of the recrystallized grains. The lifetime is not changed during the recrystallization, when the change in type of the trapping sites occurs. It is not surprising as similarly to dislocations, positrons are trapped at GBs in vacancy-like defects.

The trapping rate K_D is directly correlated with the mean dislocation density ϱ_D in the non-recrystallized specimen prior recrystallization

$$\varrho_D = \frac{\eta K_D}{\nu_D}\,, \tag{8}$$

where $\nu_D = (0.3 \times 10^{-4})$ m^{2}s^{-1} [40] is the specific positron trapping rate for dislocation in Ni. From Eq. (8) we obtain $\varrho_D = 1.5 \times 10^{14}$ m^{-2} for the specimen prior to recrystallization. This value of dislocation density agrees well with $\varrho_D = 10^{14}$ m^{-2} determined for UFG Ni in Ref. [7].

The temperature dependence of the trapping rate K_v is plotted in the lower panel of Fig. 11. There is practically no change of K_v up to about 370 °C. Above this temperature K_v decreases to a lower value and above 450 °C remains approximately constant again. The mean concentration c_v of the microvoids can be calculated from the trapping rate using the following equation [10]:

$$c_v \approx (1-\eta)\,\frac{K_v}{n\nu_{1v}}\,, \tag{9}$$

where the constant ν_{1v} is the specific positron trapping rate for Ni monovacancy. As the specific trapping rate is presently not available in literature, the quantity $c_v\nu_{1v}$ is plotted in Fig. 12 as a function of annealing temperature. This quantity differs from the mean concentration of the microvoids only by the constant multiplicative factor ν_{1v}. It is clear from Fig. 12 that c_v increases in the temperature interval of 250–370 °C, i.e. during the recrystalization up to the Curie temperature. The increase of c_v is accompanied by a

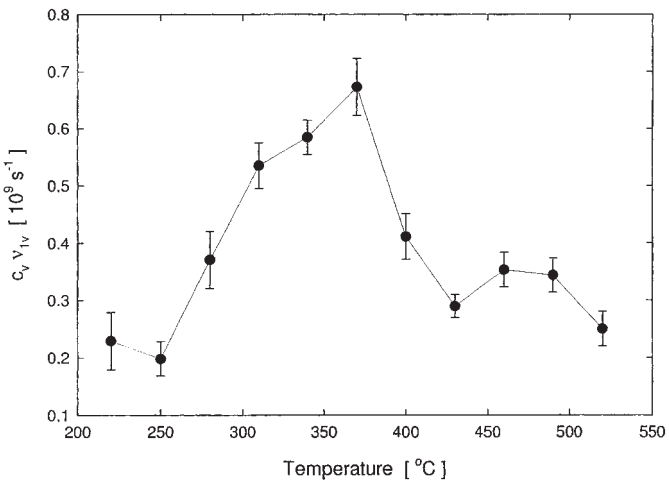

Fig. 12. Quantity $c_v\nu_{1v}$ plotted as a function of temperature. The symbol c_v means the mean concentration of the microvoids and the constant ν_{1v} stands for the specific positron trapping rate to Ni monovacancy

decrease of size of the microvoids, see Fig. 9. This behavior can be explained only as decay of larger microvoids to smaller ones. On the other hand, c_v exhibits a rapid decrease above the Curie temperature, see Fig. 12. The decrease of c_v is correlated with the increase of d_v, see Fig. 9. Hence above the Curie temperature the mean size of the microvoids increases. It may indicate that the smaller microvoids, which are not stable enough, are annealed out. Eventually above 450 °C c_v remains constant at a value, which is higher than the initial one, see Fig. 12. Some microvoids may be introduced into the specimen annealed above the Curie temperature due to the magnetostriction effect during the rapid quenching.

3.5 Comparison of PLS with other methods

As it was shown in the previous text, detailed information about processes, which take place in UFG materials with increasing temperature, can be obtained by PLS. PLS is highly sensitive to open volume defects and, therefore, allows for study of their behavior with increasing temperature. It is very interesting to compare sensitivity of various experimental techniques involved in investigations of thermal stability of UFG materials to various processes occurring in UFG specimens. The comparison of PLS with microhardness and electrical resistivity measurements [7] is shown in Fig. 13. The positron-lifetime spectra are characterized by the mean lifetime $\overline{\tau}$ in order to have a single integral parameter. Each point in Fig. 13 corresponds to some annealing temperature indicated by the value in vicinity of this point. Electrical resistivity radically decreases due to the abnormal grain growth (130–200 °C), while the recrystallization causes remarkably smaller decrease of resistivity. The mean lifetime exhibits almost opposite sensitivity: main recovery of $\overline{\tau}$ occurs due to recrystallization (200–400 °C), while the

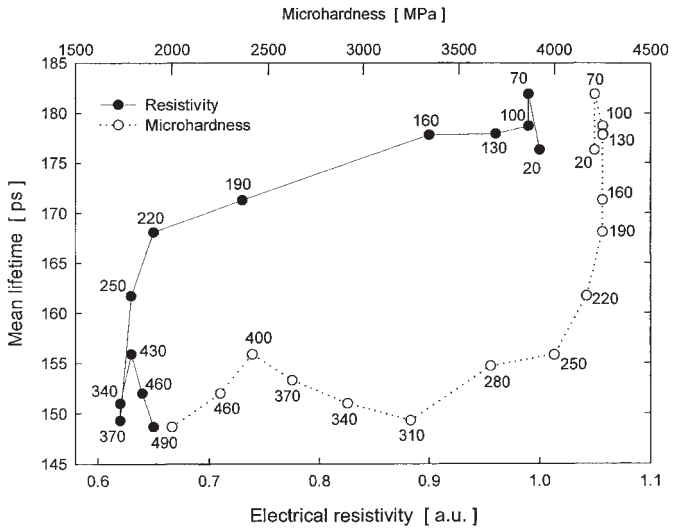

Fig. 13. Comparison of PLS with electrical resistivity and microhardness. Each point in the figure represents some annealing temperature (in °C) indicated by the value in vicinity of the point. Filled circles correspond to electrical resistivity (lower *x*-axis, in arbitrary units), while the open circles belong to microhardness (upper *x*-axis)

abnormal grain growth leads to a smaller decrease of $\bar{\tau}$, see Fig. 13. Both the electrical resistivity and the mean lifetime are sensitive to the magnetostriction phenomena, which take place due to quenching of the specimens annealed above the Curie temperature (358 °C). The abnormal grain growth practically does not affect microhardness, see Fig. 13. The recrystallization leads to a decrease of microhardness, which continues also during further growth of the recrystallized grains. The magnetostriction phenomena above the Curie temperature have no impact on microhardness, see Fig. 13.

The present comparison shows that PLS, electrical resistivity and microhardness exhibit different sensitivity to processes related with thermal recovery of UFG structure. Therefore, it is convenient to use all these techniques in investigations to obtain complementary information about thermal evolution of UFG structure.

4. Conclusions

Thermal evolution of UFG structure of Ni prepared by HPT was studied in the present work by means of PLS combined with TEM. Interpretation of PLS results was made in frame of the diffusion trapping model developed for UFG materials in Ref. [10]. The obtained results were further correlated with XRD, electrical resistivity and microhardness investigations on the same specimens [7]. The obtained results can be summarized into the following items:

(i) Positrons in UFG Ni are trapped at dislocations inside the distorted layers along GBs and in the microvoids with free volume comparable to a few vacancies. The microvoids are distributed homogeneously throughout the grains.

(ii) Up to 130 °C no structure changes detectable by PLS and TEM were found.

(iii) The abnormal grain growth, where isolated recrystallized grains grow in the deformed matrix, takes place in the temperature interval of 160–200 °C.

(iv) The recrystallization occurs from 200 to 400 °C and leads to a significant decrease of dislocation density and the volume fraction of the distorted regions. Moreover, the decay of larger microvoids to smaller ones occurs during the recrystallization.

(v) Further growth of the recrystallized grains takes place in recrystallized specimens above 400 °C.

(vi) Additional microvoids and probably also dislocations seem to be introduced into the specimen annealed above the Curie temperature (358 °C) due to the magnetostriction phenomena occuring during quenching.

Acknowledgements The residency of J. Čížek at University Göttingen was supported by the Alexander von Humboldt Foudation. The authors highly acknowledge financial support from the Grant Agency of Czech Republic (contract No. 106/01/D049) and Ministry of Education, Youth and Sport of Czech Republic within the international programme COST Action 523 (project COST OC 523.50).

References

[1] R. Z. Valiev, R. K. Islamgaliev, and I. V. Alexandrov, Prog. Mater. Sci. **45**, 103 (2000).
[2] R. Z. Valiev, Mater. Sci. Eng. A **234/236**, 59 (1998).
[3] R. Birringer, Mater. Sci. Eng. A **117**, 33 (1989).
[4] R. Z. Valiev, E. V. Kozlov, Y. F. Ivanov, J. Lian, A. A. Nazarov, and B. Baudelet, Acta Metall. Mater. **42**, 2467 (1994).

[5] R. Z. Valiev, I. V. Alexandrov, and R. K. Islamgaliev, in: Nanocrystalline Materials: Science and Technology, NATO ASI Ser., Eds. G. M. Chow and N. I. Noskova, Kluwer Academic Publ., Dordrecht 1998 (p. 121).
[6] R. Z. Valiev, A. V. Korznikov, and R. R. Mulyukov, Mater. Sci. Eng. A **168**, 141 (1993).
[7] R. K. Islamgaliev, F. Chmelík, and R. Kužel, Mater. Sci. Eng. A **237**, 43 (1997).
[8] J. Lian, R. Z. Valiev, and B. Baudelet, Acta Metall. Mater. **43**, 4165 (1995).
[9] J. Čížek, I Procházka, P. Vostrý, F. Chmelík, and R. K. Islamgaliev, Acta Phys. Pol. A **95**, 487 (1999).
[10] J. Čížek, I. Procházka, M. Cieslar, R. Kužel, J. Kuriplach, F. Chmelík, I. Stulíková, F. Bečář, O. Melikhova, and R. K. Islamgaliev, Phys. Rev. B **65**, 094106 (2002).
[11] N. M. Amirkhanov, J. J. Bucki, R. K. Islmagaliev, K. J. Kurzydlowski, and R. Z. Valiev, J. Metast. Nanostr. Mater. **9**, 21 (2001).
[12] R. K. Islamgaliev, R. Y. Murtazin, L. A. Syutina, and R. Z. Valiev, phys. stat. sol. (a) **129**, 231 (1992).
[13] P. Hautojärvi and C. Corbel, in: Proc. Internat. School Phys. 'Enrico Fermi', Course CXXV, Eds. A. Dupasquier and A. P. Mills, IOS Press, Varenna 1995 (p. 491).
[14] M. F. Imaev, Fiz. Metallov Metalloved. **64**, 824 (1987), in Russian.
[15] F. Bečvář, L. Lešták, I. Novotný, I. Procházka, F. Šebesta, and J. Vrzal, Mater. Sci. Forum **175/178**, 947 (1995).
[16] F. Bečvář, J. Čížek, L. Lešták, I. Novotný, I. Procházka, and F. Šebesta, Nucl. Instrum. Methods Phys. Res. A **443**, 557 (2000).
[17] F. Bečvář, J. Čížek, and I. Procházka, Acta Phys. Pol. A **95**, 448 (1999).
[18] I. Procházka, I. Novotný, and F. Bečvář, Mater. Sci. Forum **255/257**, 772 (1997).
[19] R. W ürschum, W. Greiner, R. Z. Valiev, M. Rapp, W. Sigle, O. Schneeweiss, and H.-E. Schaefer, Scr. Metal Mater. **25**, 2451 (1991).
[20] G. Dlubek, O. Brümmer, N. Meyendorf, P. Hautojärvi, A. Vehanen, and J. Yli-Kaupilla, J. Phys. F **9**, 1961 (1979).
[21] L. C. Smedskjaer, M. Manninen, and M. J. Fluss, J. Phys. F **10**, 2237 (1980).
[22] Y. K. Park, J. T. Waber, M. Meshii, C. L. Snead, and C. G. Park, Phys. Rev. B **34**, 823 (1986).
[23] J. Čížek, I. Procházka, T. Kmječ, and P. Vostrý, phys. stat. sol. (a) **180**, 439 (2000).
[24] K. Ueno, M. Ohmura, M. Kimura, Y. Kamimura, M. Takenaka, T. Tsutsumi, K. Ohsawa, H. Abe, and E. Kuramoto, Mater. Sci. Forum **255/257**, 430 (1997).
[25] T. E. M. Staab, R. Krause-Rehberg, and B. Kieback, J. Mater. Sci. **34**, 3833 (1999).
[26] W. B. Gauster, W. R. Wampler, W. B. Jones, J. A. Van den Avyle, in: Proc. 5th Int. Conf. Positron Annihilation, Japan 1979, Eds. R. R. Hasiguti and K. Fujiwara, The Japan Institute of Metals, Sendai 1979 (p. 1979).
[27] W. Wycisk and M. Feller-Kniepmeier phys. stat. sol. (a) **37**, 183 (1976).
[28] A. P. de Lima, C. Lopes Gil, D. R. Martins, N. Ayres de Campos, L. F. Menezes, and J. V. Fernandes, in: Proc. Europ. Meet. Positron Studies of Defects, Vol. 2, Part 1, Eds. G. Dlubek, O. Brümmer, G. Brauer, and K. Hennig, Martin-Luther-Universität Halle-Wittenberg, Wernigerode 1987 (p. C1).
[29] H.-E. Schaefer, R. Würschum, R. Birringer, and H. Gleiter, Phys. Rev. B **38**, 9545 (1988).
[30] M. Eldrup, P. G. Sanders, and J. R. Weertman, Mater. Sci. Forum **255/257**, 436 (1997).
[31] R. Würschum, M. Scheytt, and H.-E. Schaefer, phys. stat. sol. (a) **102**, 119 (1987).
[32] J. Kuriplach, S. Van Petegem, M. Hou, E. E. Zhurkin, H. Van Swygenhoven, F. Dalla Torre, G. Van Tendeloo, M. Yandouzi, D. Schryvers, D. Segers, A. L. Morales, S. Ettaoussi, C. Dauwe, Mater. Sci. Forum, in press.
[33] A. Seger and F. Banfart, phys. stat. sol. (a) **102**, 171 (1987).
[34] S. Van Petegem, J. Kuriplach, M. Hou, E. E. Zhurkin, D. Segers, A. L. Morales, S. Ettaoussi, C. Dauwe, and W. Mondelaers, Mater. Sci. Forum, in press.
[35] J. Čížek, PhD Thesis, Charles University, Prague, 2001.
[36] F. von Göhler and G. Sachs, Z. Phys. **77**, 281 (1932).
[37] M. Avrami, J. Chem. Phys. **7**, 1103 (1939).
[38] H. Margolin (Ed.) Recrystallization, Grain Growth and Textures, American Society for Metals, Metals Park, Ohio 1966 (p. 231).
[39] G. Dlubek, Mater. Sci. Forum **13/14**, 15 (1987).
[40] R. M. Nieminen, and M. J. Manninen, in: Positrons in Solids, Ed. P. Hautojärvi, Springer-Verlag, Berlin 1979 (p. 145).